

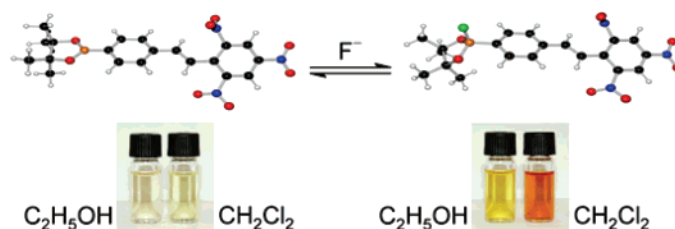
Nitro-Substituted Stilbeneboronate Pinacol Esters and Their Fluoro-Adducts. Fluoride Ion Induced Polarity Enhancement of Arylboronate Esters

Alexander Oehlke,[†] Alexander A. Auer,[‡] Ina Jahre,[‡] Bernhard Walfort,[§] Tobias Rüffer,[§] Petra Zoufalá,[§] Heinrich Lang,[§] and Stefan Spange^{*,†}

Department of Polymer Chemistry, Department of Theoretical Chemistry, and Department of Inorganic Chemistry, Institute of Chemistry, Chemnitz University of Technology, Strasse der Nationen 62, 09111 Chemnitz, Germany

stefan.spange@chemie.tu-chemnitz.de

Received January 15, 2007



A series of stilbeneboronate pinacol cyclic esters, containing none to three nitro groups, have been synthesized by various olefination reactions and characterized by X-ray single-crystal structure analysis. A stilbeneboronate ester bearing electron-acceptor groups experiences transition to a push–pull π -electron system upon complexation with one fluoride ion at the boron atom. The UV–vis absorption maxima of the presented nitro-substituted stilbeneboronate esters are red-shifted upon addition of fluoride ions, indicating this binding event. The enhancement of the polarity of the investigated compounds and the changes in the electronic system were investigated by UV–vis absorption spectroscopy and solvatochromism. Additionally, studies were performed by natural bond orbital (NBO) analysis and RI-CC2 calculations of the vertical excitation energies. The synergism of fluoride ion complexation and solvation upon the UV–vis band shift is interpreted in terms of linear solvation energy relationships (LSERs) using the Kamlet–Taft solvent parameter set. It is found that the UV–vis absorption of the fluoro-boronates is strongly dependent on the solvents hydrogen-bond donating ability.

Introduction

Arylboronic acids and arylboronate esters, known as building blocks for a variety of coupling reactions,¹ i.e., Suzuki cross-coupling,^{1a} are also well-established compounds for the detection of carbohydrates² as a result of their ability to reversibly form cyclic esters with appropriate diols.³ Several π -chromophoric

compounds with a boron moiety not directly bound to the chromophore have been prepared, i.e., colorimetric internal charge-transfer (ICT) carbohydrate sensors.⁴ A large number of chromophoric compounds containing sp^2 -hybridized boron moieties directly bound to a conjugated π -electron system were synthesized during the past decade.^{5–10} Derivatives of arylboronic acids, arylboronate esters, and triarylboranes belong to these classes of compounds in which the vacant p-orbital of

[†] Department of Polymer Chemistry.

[‡] Department of Theoretical Chemistry.

[§] Department of Inorganic Chemistry.

(1) (a) Miyaura, N.; Suzuki, A. *Chem. Rev.* **1995**, *95*, 2457–2483. (b) Ley, S.; Thomas, A. *Angew. Chem. Int. Ed.* **2003**, *42*, 5400–5449.

(2) For reviews on carbohydrate detection, see: (a) James, T.; Sandanayake, K.; Shinkai, S. *Angew. Chem., Int. Ed.* **1996**, *35*, 1910–1922. (b) James, T.; Shinkai, S. *Top. Curr. Chem.* **2002**, *218*, 159–200. (c) Wang, W.; Gao, X.; Wang, B. *Curr. Org. Chem.* **2002**, *6*, 1285–1317. (d) Striegler, S. *Curr. Org. Chem.* **2003**, *7*, 81–102. (e) James, T. In *Boronic Acids*; Hall, D., Ed.; Wiley-VCH: Weinheim, 2005; pp 441–479.

(3) (a) Kuivila, H.; Keough, A.; Soboczenski, E. *J. Org. Chem.* **1954**, *19*, 780–783. (b) Lorand, J.; Edwards, J. *J. Org. Chem.* **1959**, *24*, 769–774.

(4) (a) Sandanayake, K.; Shinkai, S. *J. Chem. Soc., Chem. Commun.* **1994**, 1083–1084. (b) Ward, C.; Patel, P.; Ashton, P.; James, T. *Chem. Commun.* **2000**, 229–230. (c) Ward, C.; Patel, P.; James, T. *J. Chem. Soc., Perkin Trans. 1* **2002**, 462–470. (d) Ward, C.; Patel, P.; James, T. *Org. Lett.* **2002**, *4*, 477–479.

(5) DiCesare, N.; Lakowicz, J. *Org. Lett.* **2001**, *3*, 3891–3893.

the boron atom participates in the aromatic system. Azo compounds,⁵ Schiff bases,⁶ stilbenes,⁷ and related compounds⁸ were reported with directly bound boronic acid or boronate ester moieties. Derivatives of triarylboranes that are essential components of chromophoric π -systems (stilbenes, biphenyls, acetylenes, thiophene derivatives)^{9,10} have been also well established as new materials in the field of organic light-emitting devices (OLED),⁹ optoelectronic, and two-photon materials.¹⁰ Another scope of application of boron-containing chromophoric π -systems is the area of selective anion sensing.¹¹ Intensive research was focused on the field of non-boron-containing fluoride ion sensors that is especially based on the strong hydrogen-bond accepting ability of the fluoride ion.¹² However, fluoride ion sensing with organoboron compounds is still a promising field of science, including arylboronic acids, arylboronate esters, and arylboranes.^{13–16} The strong interaction of three-coordinate boron compounds as “hard” Lewis acids and fluoride ions as “hard” Lewis bases is one of the origins for the high selectivity of boron-containing sensing materials toward

fluoride ions. Hitherto manifold detection methods were developed utilizing different fluoride-driven responses. These approaches use changes of the fluorescence¹³ and the colorimetric^{13d,14} behavior. Also fluoride sensors based on redox reactions^{9j,15} and probes using phosphorescence¹⁶ were reported. Furthermore, sensors based on boron-containing subphthalocyanines are known.¹⁷ In addition, approaches related to fluoride-sensing exist for the detection of cyanide ions.^{17a,18} Arylboronic acids are mostly reported as boron-containing fluoride sensors, but they show multiple equilibria due to the formation of various fluoroborate species.^{13a,b,g} They also have the disposition to form cyclic boroxines, which implies difficulties during syntheses and analyses. These disadvantages can be circumvented by the utilization of arylboronate esters^{13e,f,h,15c} as protecting groups such as pinacol cyclic esters.^{13h}

The coordination of Lewis bases such as amines,¹⁹ F^- , HO^- , and CN^- at the planar boron atom alters the hybridization from sp^2 to sp^3 and, hence, changes the electronic character. Up to now, Hammett constant characteristics of the electronic effect of boron-containing substituents are rarely reported for related types of moieties including sp^2 and sp^3 -hybridized boron atoms.²⁰ This is particularly true for fluoro-adducts of arylboronate esters. To display the difference between the electronic effects of the two different states of hybridization, the Hammett constants of the boronic acid moiety $-B(OH)_2$ ($\sigma_p = 0.12$; $\sigma_m = -0.01$)²⁰ and its boronate form $-B(OH)_3^-$ ($\sigma_p = -0.44$; $\sigma_m = -0.48$)²⁰ can be taken into account. However, the latter form is marked as a group with one of the highest field effects/inductive effects ($F = -0.42$).²⁰ This effect can also be applied to arylboronate esters and their fluoride adducts, but the exact values will surely differ from the aforementioned ones. The σ_p and σ_m constants of alkyl esters of boronic acids as substituent,

(6) (a) Norman, D.; Edwards, J.; Vogels, C.; Decken, A.; Westcott, S. *Can. J. Chem.* **2002**, *80*, 31–40. (b) Vogels, C.; Nikolcheva, L.; Norman, D.; Spinney, H.; Decken, A.; Baerlocher, M.; Baerlocher, F.; Westcott, S. *Can. J. Chem.* **2001**, *79*, 1115–1123. (c) Zhang, H.; Norman, D.; Wentzell, T.; Irving, A.; Edwards, J.; Wheaton, S.; Vogels, C.; Westcott, S. *Transition Met. Chem.* **2005**, *30*, 63–68.

(7) (a) Shimori, H.; Takeuchi, M.; Shinkai, S. *Tetrahedron* **1995**, *51*, 1893–1902. (b) DiCesare, N.; Lakowicz, J. *J. Photochem. Photobiol. A* **2001**, *143*, 39–47. (c) DiCesare, N.; Lakowicz, J. *J. Phys. Chem. A* **2001**, *105*, 6834–6840. (d) Baumgarten, M.; Yüksel, T. *Phys. Chem. Chem. Phys.* **1999**, *1*, 1699–1706. (e) Larsen, M.; Krebs, F.; Jørgensen, M.; Harrit, N. *J. Org. Chem.* **1998**, *63*, 4420–4424.

(8) (a) DiCesare, N.; Lakowicz, J. *Chem. Commun.* **2001**, 2022–2023. (b) Sato, K.; Sone, A.; Arai, S.; Yamagishi, T. *Heterocycles* **2003**, *61*, 31–38. (c) Badugu, R.; Lakowicz, J.; Geddes, C. *Anal. Chem.* **2004**, *76*, 610–618.

(9) (a) Yamaguchi, S.; Shirasaka, T.; Tamao, K. *Org. Lett.* **2000**, *2*, 4129–4132. (b) Jia, W.; Song, D.; Wang, S. *J. Org. Chem.* **2003**, *68*, 701–705. (c) Jia, W.; Bai, D.; McCormick, T.; Liu, Q.; Motala, M.; Wang, R.; Seward, C.; Tao, Y.; Wang, S. *Chem. Eur. J.* **2004**, *10*, 994–1006. (d) Jia, W.; Moran, M.; Yuan, Y.; Hong Lu, Z.; Wang, S. *J. Mater. Chem.* **2005**, *15*, 3326–3333. (e) Mazzeo, M.; Vitale, V.; Della Sala, F.; Anni, M.; Barbarella, G.; Favaretto, L.; Sotgiu, G.; Cingolani, R.; Gigli, G. *Adv. Mater.* **2005**, *17*, 34–39. (f) Jia, W.; Feng, X.; Bai, D.; Lu, Z.; Wang, S.; Vamvounis, G. *Chem. Mater.* **2005**, *17*, 164–170. (g) Stahl, R.; Lambert, C.; Kaiser, C.; Wortmann, R.; Jakober, R. *Chem. Eur. J.* **2006**, *12*, 2358–2370. (h) Lequan, M.; Lequan, R.; Chane-Ching, K.; Callier, A. *Adv. Mater. Opt. Electron.* **1992**, *1*, 243–247. (i) Yamaguchi, S.; Akiyama, S.; Tamao, K. *J. Am. Chem. Soc.* **2000**, *122*, 6335–6336. (j) Nicolas, M.; Fabre, B.; Marchand, G.; Simonet, J. *Eur. J. Org. Chem.* **2000**, 1703–1710.

(10) (a) Liu, Z.; Fang, Q.; Wang, D.; Cao, D.; Xue, G.; Yu, W.; Lei, H. *Chem. Eur. J.* **2003**, *9*, 5074–5084. (b) Liu, Z.; Fang, Q.; Cao, D.; Wang, D.; Xu, G. *Org. Lett.* **2004**, *6*, 2933–2936. (c) Liu, Z.; Shi, M.; Li, F.; Fang, Q.; Chen, Z.; Yi, T.; Huang, C. *Org. Lett.* **2005**, *7*, 5481–5484. (d) Cao, D.; Liu, Z.; Fang, Q.; Xu, G.; Xue, G.; Liu, G.; Yu, W. *J. Organomet. Chem.* **2004**, *689*, 2201–2206. (e) Charlot, M.; Porres, L.; Entwistle, C.; Beeby, A.; Marder, T.; Blanchard-Desce, M. *Phys. Chem. Chem. Phys.* **2005**, *7*, 600–606. (f) Yuan, Z.; Entwistle, C.; Collings, J.; Albesa-Jové, D.; Batsanov, A.; Howard, J.; Taylor, N.; Kaiser, H.; Kaufmann, D.; Poon, S.; Wong, W.; Jardin, C.; Fathalla, S.; Boucekkine, A.; Halet, J.; Marder, T. *Chem. Eur. J.* **2006**, *12*, 2758–2771.

(11) For reviews on anion sensing see: (a) de Silva, A.; Gunaratne, H.; Gunnlaugsson, T.; Huxley, A.; McCoy, C.; Rademacher, J.; Rice, T. *Chem. Rev.* **1997**, *97*, 1515–1566. (b) Beer, P.; Gale, P. *Angew. Chem. Int. Ed.* **2001**, *40*, 486–516. (c) Martinez-Manez, R.; Sancenon, F. *Chem. Rev.* **2003**, *103*, 4419–4476.

(12) (a) Boiocchi, M.; Del Boca, L.; Esteban-Gomez, D.; Fabbri, L.; Licchelli, M.; Monzani, E. *J. Am. Chem. Soc.* **2004**, *126*, 16507–16514. (b) Pohl, R.; Aldakov, D.; Pavel, K.; Jursikova, K.; Marquez, M.; Anzenbacher, P. *Chem. Commun.* **2004**, 1282–1283. (c) Cho, E.; Ryu, B.; Lee, Y.; Nam, K. *Org. Lett.* **2005**, *7*, 2607–2609. (d) Peng, X.; Wu, Y.; Fan, J.; Tian, M.; Han, K. *J. Org. Chem.* **2005**, *70*, 10524–10531. (e) Esteban-Gomez, D.; Fabbri, L.; Licchelli, M. *J. Org. Chem.* **2005**, *70*, 5177–5172. (f) Lin, Z.; Ou, S.; Duan, C.; Zhang, B.; Bai, Z. *Chem. Commun.* **2006**, 624–626.

(13) (a) Cooper, C.; Spencer, N.; James, T. *Chem. Commun.* **1998**, 1365–1366. (b) DiCesare, N.; Lakowicz, J. *Anal. Biochem.* **2002**, *301*, 111–116. (c) Yamaguchi, S.; Shirasaka, T.; Akiyama, S.; Tamao, K. *J. Am. Chem. Soc.* **2002**, *124*, 8816–8817. (d) Kubo, Y.; Yamamoto, M.; Ikeda, M.; Takeuchi, M.; Shinkai, S.; Yamaguchi, S.; Tamao, K. *Angew. Chem., Int. Ed.* **2003**, *42*, 2036–2040. (e) Arimori, S.; Davidson, M.; Fyles, T.; Hibbert, T.; James, T.; Kociok-Köhn, G. *Chem. Commun.* **2004**, 1640–1641. (f) Kubo, Y.; Kobayashi, A.; Ishida, T.; Misawa, Y.; James, T. *Chem. Commun.* **2005**, 2846–2848. (g) Badugu, R.; Lakowicz, J.; Geddes, C. *Sens. Actuators, B* **2005**, *104*, 103–110. (h) Neumann, T.; Dienes, Y.; Baumgartner, T. *Org. Lett.* **2006**, *8*, 495–497. (i) Shiratori, H.; Ohno, T.; Nozaki, K.; Osuka, A. *Chem. Commun.* **1999**, 2181–2182. (j) Liu, X.; Bai, D.; Wang, S. *Angew. Chem., Int. Ed.* **2006**, *45*, 5475–5478. (k) Parab, K.; Venkatasubbiah, K.; Jäkle, F. *J. Am. Chem. Soc.* **2006**, *128*, 12879–12885. (l) Yuchi, A.; Tatebe, A.; Kani, S.; James, T. *Bull. Chem. Soc. Jpn.* **2001**, *74*, 509–510. (m) Swamy, K.; Ju Lee, Y.; Na Lee, H.; Chun, J.; Kim, Y.; Kim, S.; Yoon, J. *J. Org. Chem.* **2006**, *71*, 8626–8628.

(14) (a) Ward, C.; Patel, P.; James, T. *Chem. Lett.* **2001**, 406–407. (b) Yamaguchi, S.; Akiyama, S.; Tamao, K. *J. Am. Chem. Soc.* **2001**, *123*, 11372–11375. (c) Yamaguchi, S.; Akiyama, S.; Tamao, K. *J. Organomet. Chem.* **2002**, *652*, 3–9. (d) Sole, S.; Gabbai, F. *Chem. Commun.* **2004**, 1284–1285. (e) Hudnall, T.; Melaimi, M.; Gabbai, F. *Org. Lett.* **2006**, *8*, 2747–2749.

(15) (a) Dusemund, C.; Sandanayake, K.; Shinkai, S. *J. Chem. Soc., Chem. Commun.* **1995**, 333–334. (b) Yamamoto, H.; Ori, A.; Ueda, K.; Dusemund, C.; Shinkai, S. *Chem. Commun.* **1996**, 407–408. (c) Aldridge, S.; Bresner, C.; Fallis, I.; Coles, S.; Hursthouse, M. *Chem. Commun.* **2002**, 740–741.

(16) Melaimi, M.; Gabbai, F. *J. Am. Chem. Soc.* **2005**, *127*, 9680–9681. (17) (a) Ros-Lis, J.; Martinez-Manez, R.; Soto, J. *Chem. Commun.* **2005**, 5260–5262. (b) Xu, S.; Chen, K.; Tian, H. *J. Mater. Chem.* **2005**, *15*, 2676–2680.

(18) (a) Badugu, R.; Lakowicz, J.; Geddes, C. *J. Am. Chem. Soc.* **2005**, *127*, 3635–3641. (b) Badugu, R.; Lakowicz, J.; Geddes, C. *Dyes Pigm.* **2005**, *64*, 49–55.

(19) (a) Bosch, L.; Fyles, T.; James, T. *Tetrahedron* **2004**, *60*, 11175–11190. (b) Zhu, L.; Shabbir, S.; Gray, M.; Lynch, V.; Sorey, S.; Ansllyn, E. *J. Am. Chem. Soc.* **2006**, *128*, 1222–1232 and references therein.

(20) Hansch, C.; Leo, A.; Taft, R. *Chem. Rev.* **1991**, *91*, 165–195.

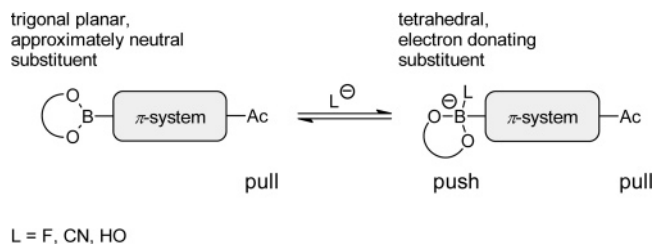


FIGURE 1. An arylboronate ester unit and an electron acceptor (Ac) are located at the same π -system. Change of hybridization of boron upon complexation with a Lewis base (L) led to the formation of a CT enhanced push–pull π -electron system.

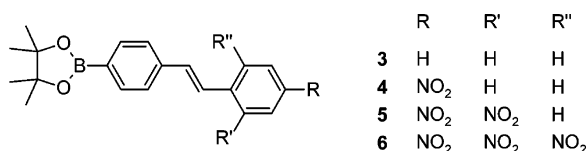


FIGURE 2. Molecular structure of the investigated stilbeneboronate esters **3–6**.

including the pinacolboronate unit, approach zero, as can be seen by $\sigma_p = 0.04$ and $\sigma_m = 0.01$ for the dimethoxyboronate unit $-B(OMe)_2$.²⁰ These substituents can therefore be considered as approximately neutral. The presence of electron-accepting groups such as $-NO_2$ and a boronate ester moiety at the same chromophore can be considered as a pull π -electron system, which is therefore changed to a push–pull π -electron system upon complexation with fluoride. As a consequence of this binding event an enhanced charge-transfer (CT) interaction between the anionic arylboronate ester and the acceptor groups (Figure 1) is observable.^{7c}

In this paper we report on the influence of the polarity enhancement of a boron moiety directly bound to a chromophoric π -electron system. For this work we have synthesized a series of stilbeneboronate pinacol cyclic esters bearing none, one, two, or three nitro groups as electron acceptors to adjust the acceptor strength (Figure 2).

It is suggested that the pull π -electron system will be transformed to a push–pull π -system showing CT effects noticeable by a corresponding bathochromic shift of its UV–vis absorption maximum. The complex formation at the boron atom will be performed with n -Bu₄NF (TBAF) as fluoride ion source. The solvatochromism of the arylboronate esters as well as the fluoro-boronate adducts has been studied to show the influence of synergism of solvent interactions and fluoride ion complexation upon the chromophoric system. The geometries of the four stilbeneboronate pinacol esters and the corresponding fluoro-adducts were optimized with DFT methods at the B3-LYP/TZVP level of theory. Their electronic structure has been investigated by means of natural bond orbital (NBO) analysis and the optical properties by CC2 response calculations.

Results and Discussion

Synthesis of Substituted (*E*)-Stilbeneboronate Pinacol Esters. As shown in Scheme 1, the synthesis of compounds **3–6** starts with the protection of 4-formylbenzeneboronic acid (**1**) with pinacol in dry diethyl ether.^{9j,21} The resulting pinacol ester **2** is converted via Horner–Wadsworth–Emmons reaction

with the appropriate diethylphosphonates to the stilbeneboronate pinacol esters **3** and **4**. Compound **5** was obtained by Knoevenagel condensation of **2** with 2,4-dinitrophenylacetic acid using catalytic amounts of piperidine. Rozhkov and co-workers at last reported the well-known reaction of 2,4,6-trinitrotoluene (TNT) with aromatic aldehydes.²² A modified procedure was applied for the synthesis of the substituted trinitrostilbene **6** by using catalytic amounts of piperidine. Use of equimolar amounts of piperidine should be avoided because of the formation of piperidine-boron adducts or Meisenheimer-analogue intermediates. As both obstacles represent equilibria reactions, catalytic amounts of the applied base are required for the respective reaction. Compounds **3** and **6** were obtained in good yields, while the yields of **4** and **5** are only 31% and 21%, respectively. The exclusive *trans*-configuration of the central C=C double bond of **3–6** in solution is shown by the coupling constant $^3J_{HH}$, which is around 16.3 Hz for all stilbenes. ¹H and ¹³C NMR spectra are consistent with the molecular structure of **3–6**. The signal for the carbon atom directly bound to the boron atom is not observed because of line broadening as a result of the quadrupole moment of ¹¹B. The chemical shifts observed for ¹¹B at about $\delta = 30$ ppm are typical values for arylboronate pinacol esters.^{6b,13h}

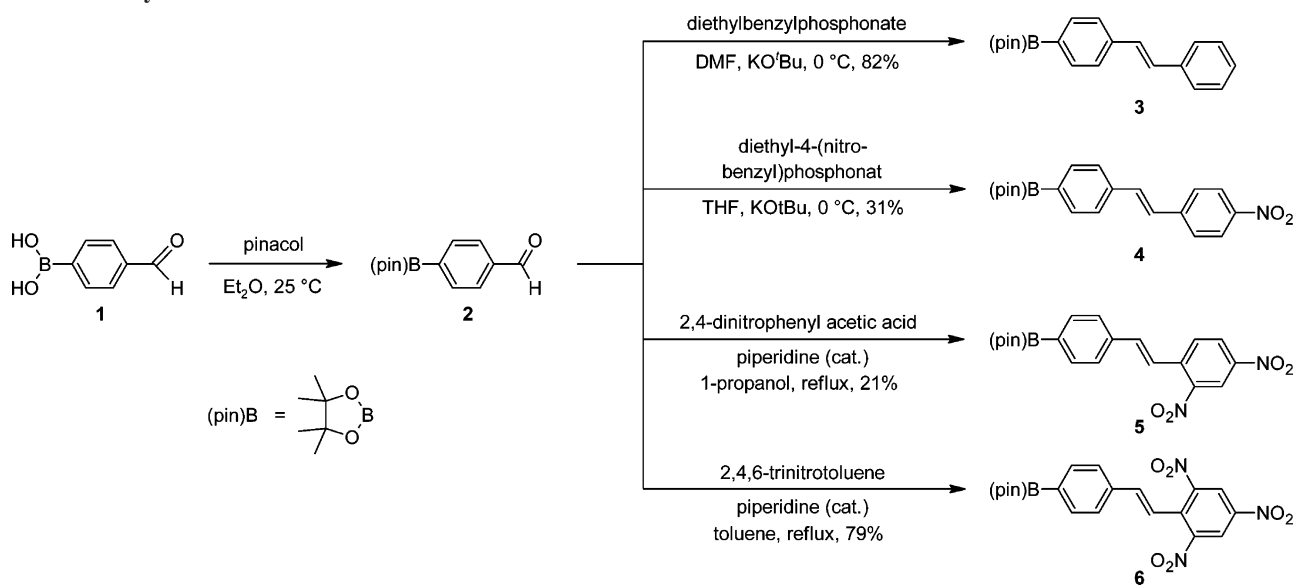
X-ray Single-Crystal Structure Analysis. The molecular structures of the (*E*)-stilbeneboronate pinacol esters **3–6** could be determined by X-ray crystallography. The crystallographic data and collection parameters as well as ORTEP plots of **3–6** are provided as Supporting Information. The presence of a central *trans* C=C double bond in the crystalline state is displayed for all four compounds. There are two independent molecules in the asymmetric unit for **3** and **5**. There is a trend toward a slightly longer central C=C double bond (C7–C8) with an increasing number of nitro groups bound at the stilbene unit referring to a higher degree of quinoidal resonance structures. Experimental bond lengths are consistent with those obtained from DFT calculations (see below). Selected bond lengths and torsions angles are compared with computed DFT values in Table 3.

Fluoro-Boronate Adducts. The fluoro-boronate adducts were generated by adding TBAF (1 M in THF or 0.1 M in THF) to freshly prepared solutions of the stilbenes **3–6**. The formation of the respective fluoro-boronate species was monitored by ¹¹B NMR spectroscopy. Upon gradual addition of TBAF to stoichiometric amounts of the stilbenes the ¹¹B signal at ca. 30 ppm disappears, and a new signal at ca. 5 ppm is observed, which is typical for tetrahedral coordinated fluoro-pinacolboronate species.^{9j,13h} The selectivity of boron compounds toward fluoride ions was reported in the literature for several examples.^{13h,15a} Small changes of the UV–vis absorption of **6** were observed by addition of n -Bu₄NCl. Addition of bromide or iodide ions, in form of their n -Bu₄N⁺ salts, to **3–6** did not change their UV–vis absorption. The formation of an anionic fluoro-boronate species refers to an enhancement of the polarity from an approximately neutral boron unit to an electron-donating group (Figure 3). The interaction of the generated electron-donating group through the polarizable stilbene π -system with an electron-withdrawing group leads to the formation of a CT enhanced push–pull π -electron system. The resulting changes

(21) Koolmeister, T.; Södergren, M.; Scobie, M. *Tetrahedron Lett.* **2002**, *43*, 5965–5968.

(22) (a) Rozhkov, V.; Kuvshinov, A.; Gulevskaya, V.; Chervin, I.; Shevelev, S. *Synthesis* **1999**, *12*, 2065–2070. (b) Splitter, J.; Calvin, M. *J. Org. Chem.* **1955**, *20*, 1086–1115.

(23) Fischer, K.; Prause, S.; Spange, S.; Cichos, F.; von Borczyskowski, C. *J. Polym. Sci., Part B: Polym. Phys.* **2003**, *41*, 1210–1218.

SCHEME 1. Synthesis of Substituted Stilbeneboronate Esters 3–6^a

of the electronic properties, which occur upon complexation with one fluoride ion, can easily be observed by UV–vis absorption spectroscopy (Figure 4). Corresponding UV–vis absorption maxima are given in Table 1.

With the increasing number of nitro groups bound at the stilbene unit (increasing acceptor strength) the UV–vis absorption maximum measured in the nonpolar solvent cyclohexane is shifted to longer wavelengths, as can be seen from Table 1. Compounds **5** and **6** measured in dichloromethane show the same UV–vis absorption maximum caused by small but slightly different solvatochromic effects (see below). The generation of the fluoro-boronate species was performed in dichloromethane solutions of the investigated stilbenes **3–6**, due to the insolubility of TBAF in nonpolar solvents such as cyclohexane and *n*-hexane, respectively. A bathochromic shift of the UV–vis absorption band can be observed upon addition of TBAF to **4–6**. Compound **3** shows only minimal spectral changes upon addition of TBAF. Its UV–vis absorption maximum is not shifted to longer wavelengths, due to the absence of a push–pull π -electron system. The fluoride ion induced red shift of the UV–vis absorption increases from **4/4•F⁻** ($\Delta\lambda_{\text{max}} = 27$ nm; $\Delta\tilde{\nu}_{\text{max}} = 1991$ cm⁻¹) to **5/5•F⁻** ($\Delta\lambda_{\text{max}} = 47$ nm; $\Delta\tilde{\nu}_{\text{max}} = 3109$ cm⁻¹) and **6/6•F⁻** ($\Delta\lambda_{\text{max}} = 66$ nm; $\Delta\tilde{\nu}_{\text{max}} = 4174$ cm⁻¹). This is caused by increasing the strength of the push–pull π -electron system with the growing number of nitro groups at the acceptor unit of the stilbene chromophore (increased acceptor strength).

Gradual addition of fluoride ions to **4–6** (illustrated in Figures 5–7) allows the determination of binding constants.^{14d,24} The coordination of one fluoride ion to the respective stilbeneboronate esters is clearly seen by the titration curves (see Supporting Information). UV–vis titration experiments in dichloromethane at 25 °C yielded different fluoride binding constants for **4** ($1.9(0.3) \times 10^5$ M⁻¹), **5** ($3.8(0.4) \times 10^5$ M⁻¹), and **6** ($5.3(0.8) \times 10^5$ M⁻¹), which corresponds to the growing acceptor strength with the growing number of nitro groups. The larger the electron-withdrawing character of the acceptor group, the larger the electrophilicity of the stilbeneboronate pinacol esters. Related

results were reported for stilbeneboronic acids by DiCesare and Lakowicz.^{13b} The calculated binding constants for the boronate esters **4–6** are comparable to those determined for donor-substituted triarylboranes.^{10c,13c,d,j,14b} However, the values calculated in this work are larger than previously reported ones for the interaction of boronate esters with fluoride ions.^{13h,15c} The binding properties of all investigated nitrostilbenes correspond to a detection limit for F⁻ in the micromolar range under experimental conditions applied. According to the absorption coefficients of the fluoro-boronate species **4•F⁻**–**6•F⁻**, detection limits in the submicromolar range are possible down to 2×10^{-7} M, as estimated by the Lambert–Beer law. A comparable detection limit was reported for a B(pin)-substituted dithienophosphole system.^{13h}

Study of Solvatochromism. The nitrostilbeneboronate esters **4–6** and their fluoro-adducts **4•F⁻**–**6•F⁻** show solvatochromic effects. The extent of the solvatochromic shift $\Delta\tilde{\nu}$ for each compound is a function of the solvent polarity, given as subscript. The solvatochromic ranges observed for the fluoro-boronate species ($\Delta\tilde{\nu}_{2,2,2\text{-trifluoroethanol/HMPA}} = 2715$ cm⁻¹ (**4•F⁻**), $\Delta\tilde{\nu}_{2,2,2\text{-trifluoroethanol/THF}} = 2860$ cm⁻¹ (**5•F⁻**), $\Delta\tilde{\nu}_{2,2,2\text{-trifluoroethanol/THF}} = 3410$ cm⁻¹ (**6•F⁻**)) are larger compared to those of the stilbeneboronate esters ($\Delta\tilde{\nu}_{\text{diethylether/DMSO}} = 1110$ cm⁻¹ (**4**), $\Delta\tilde{\nu}_{\text{methanol/TCE}} = 1050$ cm⁻¹ (**5**), $\Delta\tilde{\nu}_{\text{HMPA/tetrachloromethane}} = 2250$ cm⁻¹ (**6**); see Supporting Information). However, compounds **3** and **3•F⁻** show no significant solvatochromism. To quantify individual solvation effects the simplified Kamlet–Taft equation (eq 1) was used, from which the coefficients of the individual interaction can be determined using multiple correlation analysis.²⁵

$$\tilde{\nu}_{\text{max}} = \tilde{\nu}_{\text{max},0} + a\alpha + b\beta + s\pi^* \quad (1)$$

The parameter $\tilde{\nu}_{\text{max}}$ is the longest-wavelength UV–vis absorption maximum of a compound measured in a particular solvent, $\tilde{\nu}_{\text{max},0}$ is that of a nonpolar reference environment, α is the

(24) Connors, K. A. *Binding Constants. The Measurement of Molecular Complex Stability*; John Wiley & Sons, Inc.: New York, 1987.

(25) (a) Reichardt, C. *Chem. Rev.* **1994**, *94*, 2319–2358. (b) Reichardt, C. *Solvents and Solvents effects in Organic Chemistry*, 3rd ed.; Wiley-VCH: Weinheim, 2003.

(26) Marcus, Y. *Chem. Soc. Rev.* **1993**, *22*, 409–416.

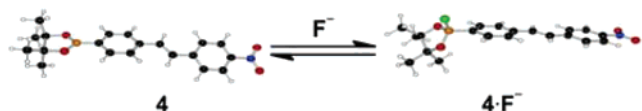


FIGURE 3. Coordination of one fluoride ion onto the pinacolboronate unit illustrated for $4/4\cdot\text{F}^-$ as their DFT optimized geometries.

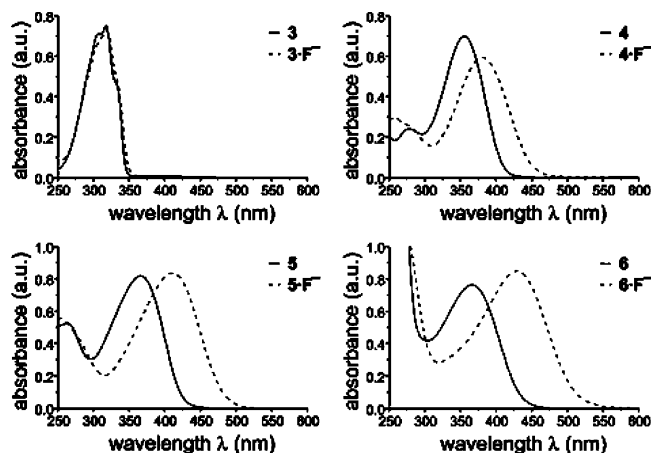


FIGURE 4. Changes in UV-vis absorption spectra of $3-6$ upon complexation with one fluoride ion measured in dichloromethane.

TABLE 1. Comparison of Experimental and Calculated UV-vis Absorption Maxima of $3-6$ and Their Fluoro-Boronate Adducts $3\cdot\text{F}^-$ – $6\cdot\text{F}^-$

	exptl λ_{max}^a (nm)	exptl λ_{max}^b (nm)	calcd λ_{max}^c (nm)	calcd λ_{max}^d (nm)
3	317	318		275
$3\cdot\text{F}^-$		318		311
4	352	355	336	296
$4\cdot\text{F}^-$		382	384	398
5	363	366	354	313
$5\cdot\text{F}^-$		413	428	449
6	371	366	370	333
$6\cdot\text{F}^-$		432	474	501

^a Measured in cyclohexane. ^b Measured in dichloromethane. ^c Calculated gas-phase values using eq 1 regarding to solvatochromism results of Table 2 (gas phase: α and β are presumed to be 0; $\pi^* = -0.8$).²³ ^d Calculated at the RI-CC2/SVP level of theory.

hydrogen-bond donating (HBD) ability, β is the hydrogen-bond accepting (HBA) ability, and π^* describes the dipolarity/polarizability of the solvent. The parameters a , b , and s are solvent-independent correlation coefficients, the sign of which indicates the direction of the shift of the UV-vis absorption maxima. The shift relates to the strength of the different solvation of the ground and the excited state of the solute.

To determine these correlation coefficients, the UV-vis absorption maxima of $4\cdot\text{F}^-$ – $6\cdot\text{F}^-$ were measured in solvents of different polarity by adding TBAF to respective solutions of $4-6$. The use of solvents is restricted owing to the lack of solubility of TBAF in nonpolar solvents. The UV-vis absorption maxima of $4-6$ are accessible in a wider range of solvents. These values are available as Supporting Information. Values of α , β , and π^* were taken from ref 26. The results of the Kamlet-Taft correlation are compiled in Table 2 for the square analyses with the best fit and significance. A representative collection of solvent-dependent UV-vis spectra of fluoro-boronate species is illustrated for $6\cdot\text{F}^-$ in Figure 8.

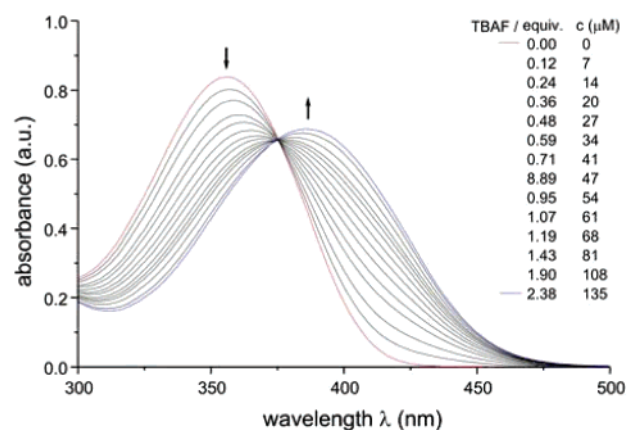


FIGURE 5. UV-vis absorption spectra of 4 ($c = 0.6 \times 10^{-4}$ M), measured in dichloromethane with different concentrations of TBAF added.

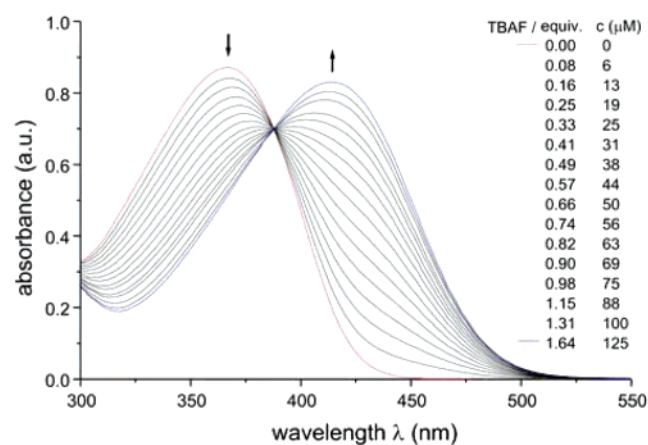


FIGURE 6. UV-vis absorption spectra of 5 ($c = 0.8 \times 10^{-4}$ M), measured in dichloromethane with different concentrations of TBAF added.

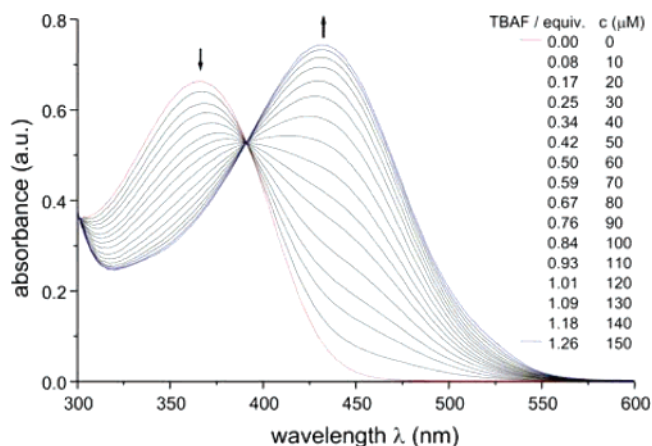


FIGURE 7. UV-vis absorption spectra of 6 ($c = 1.2 \times 10^{-4}$ M), measured in dichloromethane with different concentrations of TBAF added.

A comparison between measured and calculated $\tilde{\nu}_{\text{max}}$ values (Table 2) of the UV-vis absorption maxima of $4\cdot\text{F}^-$ – $6\cdot\text{F}^-$ is given in Figures 9–11. Clear trends are visible in the stilbeneboronate series and the fluoro-boronate series except for species $4\cdot\text{F}^-$ measured in solvents with $\alpha = 0$. The Kamlet–

TABLE 2. Solvent-Independent Correlation Coefficients a , b , and s of the Kamlet–Taft Parameters α , β , and π^* , Solute Property of the Reference System $\tilde{\nu}_{\max,0}$, Correlation Coefficient (r), Standard Deviation (SD), Number of Solvents (n) and Significance (f) for the Solvatochromism of 4–6 and 4•F[−]–6•F[−]

	$\tilde{\nu}_{\max,0}$	a	b	s	r	SD	n	f
4	28.846	0.253	0	−1.136	0.922	0.124	27	<0.0001
5	27.630	0.216	0.363	−0.728	0.863	0.156	29	<0.0001
6	27.000	0.398	1.630	0	0.903	0.306	27	<0.0001
4•F [−] ^a	26.022	1.114	0	0	0.990	0.075	11	<0.0001
4•F [−] ^b	26.285	0	−1.139	0	0.988	0.062	8	<0.0001
5•F [−]	23.860	1.761	0	0.629	0.961	0.246	17	<0.0001
6•F [−]	22.535	2.237	0	1.780	0.985	0.185	17	<0.0001

^a Measured in solvents with $\alpha > 0$ and 4-butyrolactone. ^b Measured in solvents with $\alpha = 0$.

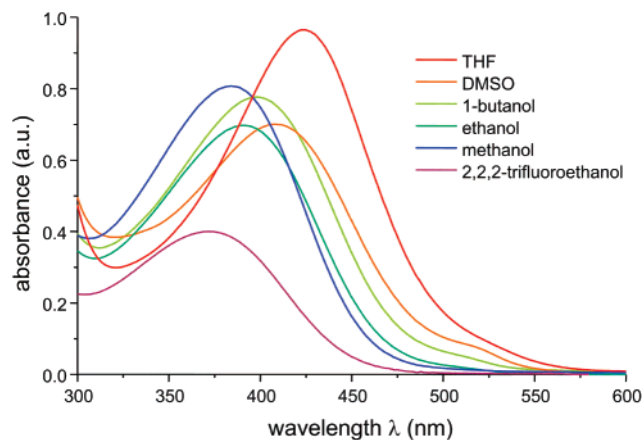


FIGURE 8. Selected UV–vis absorption spectra of 6•F[−] in six different solvents.

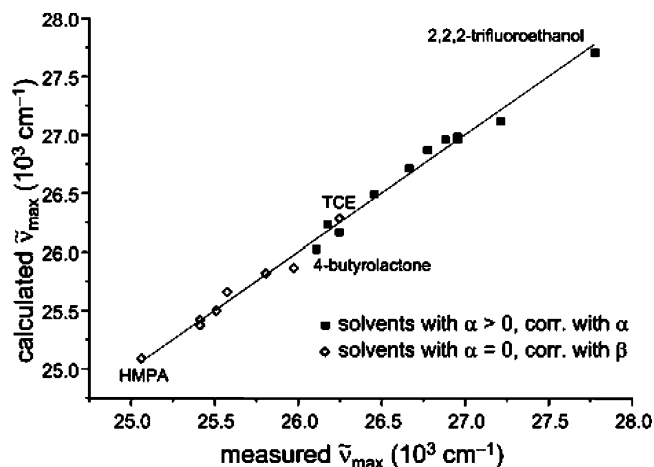


FIGURE 9. Relationship between measured and calculated ν_{\max} values for 4•F[−], measured in 11 solvents with HBD ability (■) and eight solvents without HBD ability (◇). TCE = 1,1,2,2-tetrachloroethane; HMPA = hexamethylphosphoric triamide.

Taft analysis for 4–6 describes an increasing influence of parameter β with growing number of nitro groups. This is caused by interactions of HBD solvents at the nitrostilbene unit and not as assumed at the boron center, which would yield negative values of b . The steric shielding of the boron atom by the pinacol cyclic ester is obviously large enough to prevent Lewis acid/Lewis base interactions with the solvent. The influence of parameter π^* decreases with growing number of nitro groups down to $s = 0$ for 6. The negative values of s indicate a more

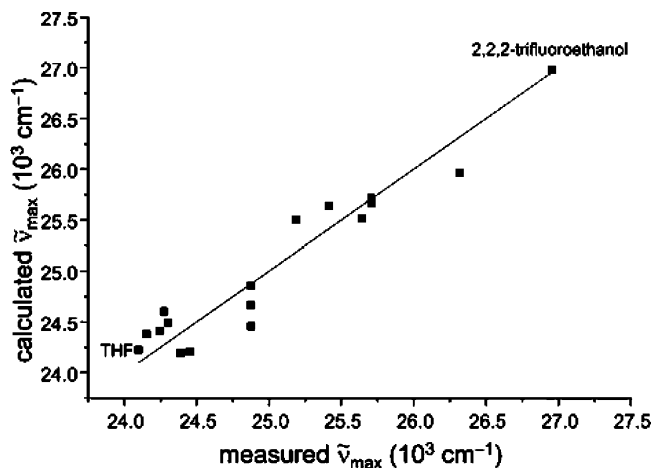


FIGURE 10. Relationship between measured and calculated ν_{\max} values for 5•F[−], measured in 17 solvents of different polarity.

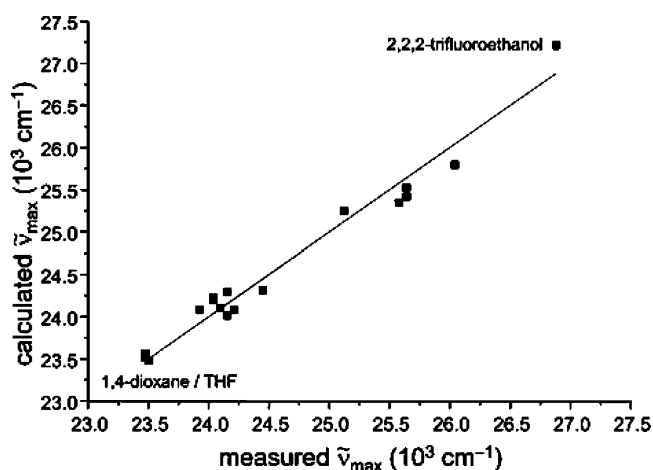


FIGURE 11. Relationship between measured and calculated ν_{\max} values for 6•F[−], measured in 17 solvents of different polarity.

polar excited state in comparison to the ground state. Furthermore, a small and steady influence of the parameter α can be observed for stilbeneboronate esters 4–6, which does not depend on the number of nitro groups within the experimental error.

The types of interactions of solvents with the solute are dramatically changed upon complexation with one fluoride ion. In comparison to 4–6 a large increase of the importance of the HBD parameter α take place for the solvatochromism of the fluoro-boronate species 4•F[−]–6•F[−]. The Kamlet–Taft correlation generally yields a strong influence of the HBD parameter α , which increases with growing number of nitro groups from 4•F[−] to 6•F[−] (Table 2). The positive value of a refers to negative solvatochromism and its origin can be interpreted as following. Solvents with HBD ability form H-bonds to the fluorine atom of the fluoro-boronate unit, and hence a decrease of electron donating to the boron atom occurs. As a consequence of subtraction of electron density at the whole fluoro-boronate unit the strength of the push–pull π -electron system of the bound chromophor is diminished and a blue shift of the UV–vis absorption results that increases with growing HBD ability of the solvent. On the other hand, solvents with HBD ability can also form H-bonds to the nitro groups, but this will cause positive solvatochromism with negative values of a in this case. The influence of the parameter π^* increases with growing

TABLE 3. Selected Calculated Bond Lengths (Å) and Torsion Angles (deg) from Geometry Optimizations of **3–6** and **3·F⁻–6·F⁻** and Selected Bond Lengths (Å) and Torsion Angles (deg) for **3–6** from X-ray Crystallography (in Italics)^a

	3 ^c	3·F⁻	4	4·F⁻	5 ^c	5·F⁻	6	6·F⁻
C4–C7	1.464 <i>1.470(3)</i>	1.461	1.460 <i>1.473(2)</i>	1.447	1.460 <i>1.470(3)</i>	1.440	1.459 <i>1.468(3)</i>	1.429
C7–C8	1.343 <i>1.313(3)</i>	1.348	1.345 <i>1.316(2)</i>	1.356	1.346 <i>1.331(3)</i>	1.364	1.345 <i>1.325(3)</i>	1.367
C8–C9	1.464 <i>1.480(3)</i>	1.456	1.462 <i>1.481(2)</i>	1.445	1.460 <i>1.463(3)</i>	1.436	1.458 <i>1.475(3)</i>	1.431
C12–B1	1.552 <i>1.548(3)</i>	1.633	1.555 <i>1.564(2)</i>	1.637	1.557 <i>1.565(3)</i>	1.636	1.558 <i>1.559(3)</i>	1.637
B1–O2	1.376 <i>1.370(2)</i>	1.480	1.374 <i>1.363(2)</i>	1.475	1.373 <i>1.360(3)</i>	1.474	1.372 <i>1.355(3)</i>	1.474
O1–B1	1.376 <i>1.365(3)</i>	1.482	1.374 <i>1.369(2)</i>	1.483	1.373 <i>1.362(3)</i>	1.475	1.373 <i>1.356(3)</i>	1.475
C3–C4–C7–C8	15.7 <i>7.9(3)</i>	9.0	13.8 <i>17.8(3)</i>	1.4	25.8 <i>-29.3(3)</i>	19.4	38.2 <i>-22.9(4)</i>	24.7
C7–C8–C9–C14	19.2 <i>-9.3(3)</i>	4.7	16.1 <i>20.9(3)</i>	1.3	12.8 <i>-2.9(4)</i>	5.9	4.6 <i>20.2(4)</i>	5.4

^a The numbering scheme corresponds to Figure S1 (see Supporting Information). Numbers in parantheses are estimated SDs in the last significant figures. Bond lengths and torsion angles of only one of the two crystallographically independent, but chemical identical, molecules are listed.

number of nitro groups starting with $s = 0$ for compound **4·F⁻**. The positive values of s indicate a more polar ground state in comparison to the excited state. This is an opposite behavior in comparison to that of **4–6**.

For species **4·F⁻** it was found that the parameter α is of importance concerning solvents with HBD ability ($\alpha > 0$) as discussed above. Solvents with no HBD ability ($\alpha = 0$) show an influence solely of the parameter β . This phenomenon is likely caused by a synergistic Lewis base interaction of such solvents and fluoride ions with the Lewis acidic arylboronate ester **4**. Both types of interaction support each other and lead to a bathochromic shift of its UV–vis absorption maximum. This is strongly supported by the fact that the UV–vis absorption maximum of **4** in the absence of fluoride ions does not show any influence on β . Beside this observation the HBA parameter β is negligible for **4·F⁻** in solvents with $\alpha > 0$, **5·F⁻**, and **6·F⁻**. This is also in contrast to the solvatochromism of **4–6**, which show a strong dependence on β .

Computational Study. To gain deeper insight into the changes of the molecular and electronic structure of the stilbeneboronate esters upon complexation with fluoride, the stilbenes **3–6** and the corresponding fluoro-boronate species **3·F⁻–6·F⁻** have been investigated. For this purpose the molecular structure, electronic density, and vertical excitation energies have been calculated using post Hartree–Fock ab initio and density functional theory methods.²⁷

Structural Parameter of the Noncomplexed and Complexed Species. As density functional theory calculations have proven to yield accurate molecular geometries, the results from quantum chemical geometry optimizations can be used to supplement experimental data, especially in cases where X-ray structural data is difficult to obtain. While experimental X-ray structural data has only been obtained for **3–6**, the equilibrium geometries for the noncomplexed (**3–6**) and their complexed species (**3·F⁻–6·F⁻**) have been obtained through geometry optimizations at the B3-LYP/TZVP level of theory.^{28,29}

The comparison between bond lengths obtained by calculation and X-ray diffraction yields root mean square (rms) deviations

of 0.013 Å for the bond lengths of all non-hydrogen atoms of **3** (0.012 Å for **4**, 0.010 Å for **5**, 0.016 Å for **6**), which is in agreement with the deviations that can be expected for the B3-LYP level of theory using basis sets of triple- ζ quality in comparison to X-ray data. As a result of packing effects in the solid state, the agreement for angles and dihedral angles is not as good, especially in the case of disordered fragments in the solid-state structure. Selected bond lengths and torsion angles as obtained from the geometry optimizations are given in Table 3 (for a complete list of calculated bond lengths between non-hydrogen atoms, see Supporting Information).

Some changes of the structure of the noncomplexed species that occur with increasing number of nitro groups at the stilbene unit should be noted. The quinoidal character of the (nitro/dinitro/trinitro)styryl unit slightly increases from **3** to **6** (C7–C8 is slightly lengthened, also shown by X-ray data; C4–C7 and C8–C9 are slightly shortened). Changes occurring at the phenyl ring directly bound to the boron atom are minimal. The B–C bond distance is slightly stretched with growing number of nitro groups. This is due to increased electron-acceptor strength, which decreases the π -electron donation from the stilbene unit to the boron atom. The B–O distances of the pinacolboronate unit slightly decrease in the same manner as a result of by π -donation from oxygen due to the larger electron deficit at the boron atom.

Structural Changes upon Complexation with F⁻. Adduct formation of boron with one fluoride ion gives an anionic fluoro-boronate species and forces the boron atom to change the state of hybridization from sp^2 to sp^3 . Therefore, structural changes are observed both at the pinacolboronate unit and the stilbene chromophore. Figure 12 gives an overview about the alterations of calculated bond lengths between non-hydrogen atoms occurring upon coordination of fluoride at the boron atom.

The most important changes take place in the π -electron system especially in the vicinity of the central C=C double bond. In general, the structures become more quinoidal upon complexation with fluoride. This can be seen by alternating lengthening and shortening of bonds of the conjugated carbon frame. So the length of the central C=C double bond increases and the bond lengths of both C–C bonds neighboring the central C=C double bond decrease. These changes are more pronounced than changes at both phenyl rings, but clear trends are

(27) Jahre, I. *Diplomarbeit*, Chemnitz University of Technology, 2006.

(28) Becke, A. D. *J. Chem. Phys.* **1993**, *98*, 5648–5652.

(29) Schäfer, A.; Horn, H.; Ahlrichs, R. *J. Chem. Phys.* **1992**, *97*, 2571–2577.

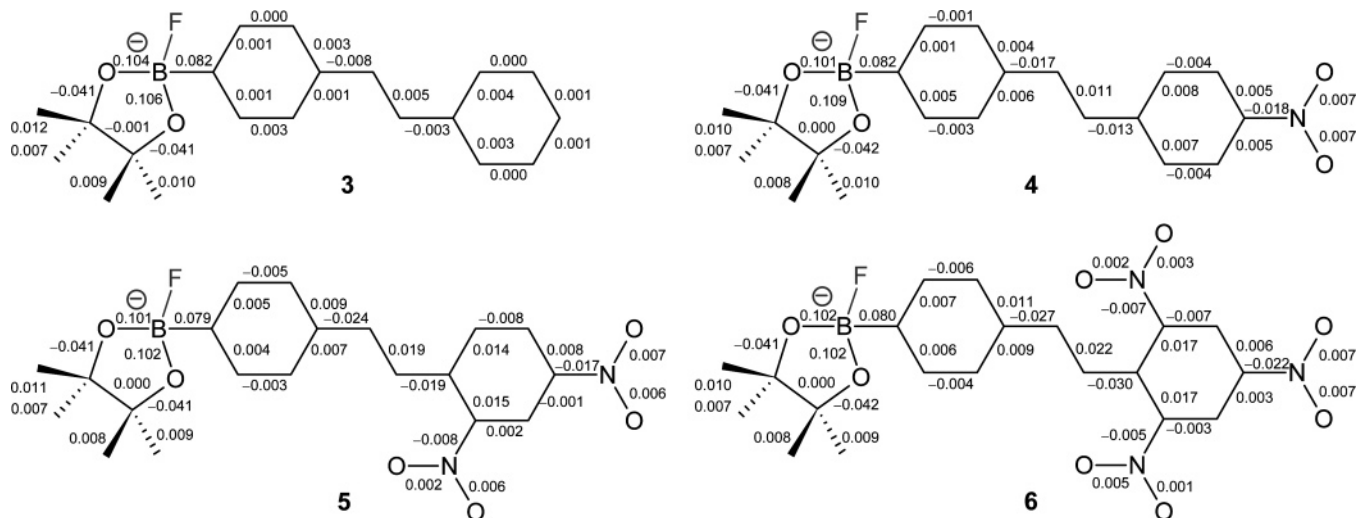


FIGURE 12. Alteration of calculated bond lengths (Å) of **3–6** upon complexation with one fluoride ion. Positive values refer to longer bond lengths upon complexation with one fluoride ion.

TABLE 4. Charges from NBO Analysis for **3–6** and **3·F⁻–6·F⁻**

subunit	3	3·F⁻	4	4·F⁻	5	5·F⁻	6	6·F⁻
NO ₂ -1			-0.27	-0.34	-0.25	-0.31	-0.23	-0.30
NO ₂ -2					-0.23	-0.28	-0.21	-0.24
NO ₂ -3							-0.19	-0.22
Ph-1	-0.01	-0.09	+0.21	+0.15	+0.36	+0.29	+0.47	+0.40
CH-1	+0.01	-0.05	0.00	-0.06	+0.02	-0.03	+0.01	-0.04
CH-2	+0.01	+0.04	+0.04	+0.07	+0.06	+0.09	+0.08	+0.11
Ph-2	-0.32	-0.36	-0.30	-0.31	-0.28	-0.25	-0.26	-0.21
B	+1.19	+1.24	+1.18	+1.24	+1.18	+1.24	+1.18	+1.24
F		-0.61		-0.61		-0.60		-0.60
O-(B)-O	-1.60	-1.73	-1.60	-1.73	-1.60	-1.73	-1.60	-1.73
CMe ₂ -CMe ₂	+0.73	+0.57	+0.73	+0.58	+0.74	+0.58	+0.74	+0.59

visible. The changes are generally larger in the order from **3·F⁻** to **6·F⁻** owing to the increasing push–pull character, i.e., the alteration of the central C=C double bond length for **6·F⁻** is around 4 times larger than that of **3·F⁻**. As can be seen by different bond length changes, the extent of conjugation of the nitro group at the para position is larger than that of the nitro groups at the ortho positions due to steric hindrance. Further changes can be observed at the pinacolboronate unit. The B–O bond distance increases, due to the absence of partial B=O double bond character, because the neighboring oxygen is not able to donate an electron pair to a tetrahedral boron. The B–C distance also increases as a result of the disruption of the resonance of boron with the π -electron system. In general, a decrease of the dihedral angles between the mean plane of both phenyl rings and the ethenyl bridge (C3–C4–C7–C8 and C7–C8–C9–C14) upon transition from **3–6** to **3·F⁻–6·F⁻** takes place (Table 3), which also conforms to an increase of the donor strength of the boronate pinacol ester unit upon complexation with fluoride.

Change of Electronic Density upon Complexation with F⁻. In order to assess the changes in the electronic structure that the four species (**3–6**) undergo upon complexation with one fluoride ion, a NBO analysis of the Kohn–Sham orbitals has been carried out for the eight molecules.³⁰ Table 4 lists the

atomic NBO charges that have been summed up for different subunits of the molecules.

In the compilation made in Table 4, which allows the quantification of the charge density redistribution, a clear trend is visible. While the electron-withdrawing influence of the nitro groups is obvious, also the influence and distribution of the additional charge from the fluoride ion can be rationalized. For all compounds the fluoride ion donates about 0.4 electrons, and the immediate effect on the boron atom is a uniform decrease of electron density for all compounds, as can be expected from the difference in electronegativity. The electron density on the neighboring oxygen atoms (O-(B)-O) altogether and the pinacol carbon scaffold (CMe₂–CMe₂) is also increased uniformly for all molecules by 10–15% of an electron owing to the decreased π -donation from oxygen to the boron atom. This is in agreement with the stretching of the B–O bond of ca. 0.1 Å for all investigated fluoro-boronate species. Smaller yet much more important changes take place in the chromophoric stilbene/nitrostilbene unit. For the nitro-substituted phenyl group

(30) For a thorough investigation of the physical significance of Kohn–Sham orbitals, see: (a) Chong, D. P.; Gritsenko, O. V.; Baerends, E. J. *J. Chem. Phys.* **2002**, *116*, 1760–1772. (b) Bickelhaupt, F. M.; Baerends, E. J. In *Reviews in Computational Chemistry*; Lipkowitz, K. B., Boyd, D. R., Eds.; Wiley-VCH: New York, 2000; Vol. 15, pp 1–86.

(31) The electron density given in Figure 13 has been calculated at the B3-LYP/TZVP level of theory. The canonical orbitals given in Figure 14 have been calculated at the HF-SCF/SVP level of theory. The figures were plotted using the gOpenmol^{32,33} and the Molden³⁴ program packages in combination with the povray raytracing tool (for details, see: <http://www.povray.org>).

(32) Laaksonen, L. *J. Mol. Graphics Modell.* **1992**, *10*, 33–34.

(33) Bergmann, D. L.; Laaksonen, L.; Laaksonen, A. *J. Mol. Graphics Modell.* **1997**, *15*, 301–306.

(34) Schaftenaar, G.; Noordik, J. H. *J. Comput.-Aided Mol. Des.* **2000**, *14*, 124–134.

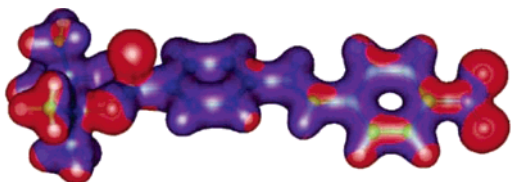


FIGURE 13. Superposition of electron density isosurfaces for neutral and complexed species shown for $4\cdot\text{F}^-$; red areas indicate regions of increased electron density, blue areas indicate regions of decreased electron density.³¹

(denoted as Ph-1) as well as for the nitro groups (NO_2 -1, NO_2 -2, NO_2 -3) themselves, an increased electron density is observed. For the bridging CH units (denoted as CH-1 and CH-2 according to the neighboring phenyl group), an increase and decrease of electron density is observed that can easily be rationalized by means of quinoidal resonance structures. For the phenyl unit neighboring the boron atom (denoted as Ph-2), an increase of electron density is observed for $3/3\cdot\text{F}^-$, little change occurs for $4/4\cdot\text{F}^-$, and a decrease of electron density is found for $5/5\cdot\text{F}^-$ and $6/6\cdot\text{F}^-$. Overall it can be concluded that the charge injected

into the conjugated π -electron system induces a further charge redistribution from the boronate ester unit, which can be regarded as an electron donor toward the nitrophenyl group acting as an electron acceptor. This is also supported by alternating lengthening and shortening of the C–C bonds. Resonance between the tetrahedral fluoro-boronate unit and the π -electron system can be neglected, and thus the observed effects are based only on the strong inductive effect of the fluoro-boronate unit. This is especially pronounced for the 2,4,6-trinitrostilbene system $6/6\cdot\text{F}^-$ that exhibits the strongest shift of the UV–vis absorption band upon complexation with one fluoride ion.

Figure 13 gives a more intuitive view on this phenomenon. In order to be able to directly compare the different electron densities, this plot shows the superposition of the electron densities of **4** and a fictitious $4\cdot\text{F}^-$ molecule that has been constructed by adding a fluoride ion at the equilibrium distance in $4\cdot\text{F}^-$ to the equilibrium structure of **4**.

This example nicely illustrates the points made in the discussion of the NBO charge analysis. While for the second phenyl unit (Ph-2) the electron density is slightly enhanced, the

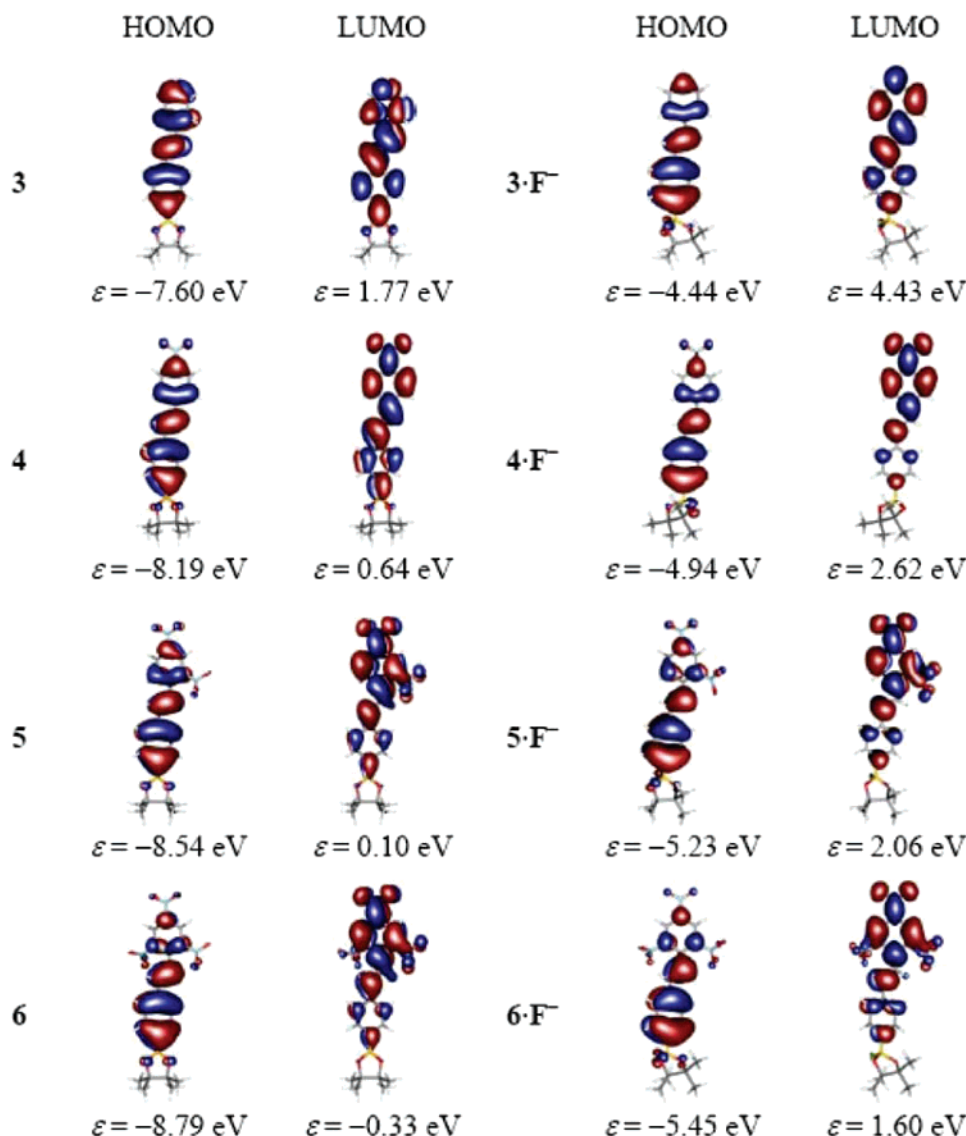


FIGURE 14. Topology of relevant orbitals of **3–6** and $3\cdot\text{F}^-$ – $6\cdot\text{F}^-$.³¹

charge density at the nitro group and the first phenyl group (Ph-1) is significantly enhanced upon complexation with fluoride.

Investigation of the Electronic Excitation Energies. In modern electronic structure theory time-dependent density functional theory (TD-DFT) methods have become a standard tool in the interpretation of optical spectra. However, while these methods have proven very reliable for many systems, one of the typical failures of TD-DFT is the correct description of charge-transfer excitations.³⁵ In such cases, ab initio methods have to be applied in order to achieve reasonable results. As recent implementations of the CC2 method³⁶ applying density fitting techniques allow such calculations for larger systems, the vertical excitation energies have been calculated using the RI-CC2 scheme as implemented by Hättig et al.³⁷

For the optical spectra of the compounds under investigation, especially of **4**·F⁻–**6**·F⁻, solvent effects play an important role. Thus, quantitative agreement of simulated spectra from the CC2 method with experimental results cannot be expected. However, the calculation of the electronic excitations can still facilitate a deeper understanding of the influence of electronic effects on excitation energies and absorption intensities. In order to estimate the residual error for these results and for comparison to TD-DFT methods, additional calculations of the vertical excitation energies have been carried out for **4**·F⁻. While the experimental value in dichloromethane solution is $\lambda_{\max} = 382$ nm and the corresponding gas-phase value according to solvatochromism results is $\lambda_{\max} = 384$ nm, the calculated vertical electronic excitation energy at the RI-CC2/TZVP level of theory correlates to $\lambda_{\max} = 411$ nm. Using the smaller, more cost-efficient SVP basis set,²⁹ the result changes marginally to $\lambda_{\max} = 398$ nm. Thus, an agreement to the experimental data within about 50 nm can be expected at the RI-CC2 level of theory. It should be pointed out that the corresponding TD-DFT result obtained at the B3-LYP/TZVP level is $\lambda_{\max} = 488$ nm. The calculated values obtained at the RI-CC2/SVP level of theory for the most intensive lines in the long-wavelength region for all of the investigated compounds are given in Table 1. The agreement with the experiment is satisfactory, a systematic error occurs most likely due to the lack of solvent effects as mentioned before. In regard to solvatochromism results the RI-CC2 calculated values of the fluoro-boronate species are larger compared to the experiment due to the nonpolar nature of the gas phase. It should be noted that the RI-CC2 results also predict an increasing shift of the most intensive absorption line upon complexation from **3**·F⁻ to **6**·F⁻ correctly, which is not the case for the TD-DFT calculations. An analysis of the dominant orbital contributions to the most intensive excitations yields deeper insight into the electronic effects that dominate the spectral features of these molecules. Generally, for the stilbeneboronate esters and the fluoro-boronate species the most intensive line in the long-wavelength region is dominated by the HOMO–LUMO transition. The topology of the corresponding orbitals is displayed in Figure 14. From a closer inspection of the orbitals it can be concluded that the effect of complexation with one fluoride ion is the more pronounced shift of charge

density upon excitation which appears to be increasing in the order **3**·F⁻ < **4**·F⁻ < **5**·F⁻ < **6**·F⁻. In the series of the fluoro-boronate adducts an increasing localization of the HOMO on the boronate ester fragment and the LUMO on the nitrophenyl fragment is observed. This finding is also in agreement with the experimental observation of the solvatochromic effects. The charge-density shift upon excitation shows the same trend as the charge-density redistribution upon complexation with fluoride.

Conclusion

A series of stilbeneboronate pinacol esters **3**–**6** bearing none to three nitro groups was prepared by olefination reactions of **2** with different CH-active compounds. X-ray single-crystal structures were obtained for stilbeneboronate pinacol cyclic esters **3**–**6**. Addition of TBAF to nitrosubstituted stilbenes leads to the formation of fluoro-pinacolboronate species representing push–pull π -electron systems. This enhancement of the polarity was studied by UV–vis spectroscopy showing bathochromic shifts of the UV–vis absorption maxima up to $\Delta\lambda_{\max} = 66$ nm for **6**·F⁻. Nitro-substituted fluoro-boronate species also show distinctive solvatochromic behavior with mainly a strong dependence of the HBD solvent parameter α .

Computational study of the molecular structures gave a good agreement with experimental X-ray single-crystal data for geometries of **3**–**6**. Structural information has also been obtained by DFT methods (B3-LYP/TZVP) for fluoro-boronate species **3**·F⁻–**6**·F⁻ not characterized by X-ray diffraction. Analysis of bond lengths and electron density indicates that complexation with one fluoride ion at the boron atom induces a charge redistribution from the arylboronate pinacol ester moiety to the nitrophenyl unit. This is especially pronounced for the fluoro-boronates that exhibit strong shifts of the UV–vis absorption maximum upon complexation. The analysis of the electronic excitations as obtained at the RI-CC2/SVP level of theory indicate that the most important excitations in the long-wavelength region are excitations in which the same bias on the charge density is present. This effect again increases from **3** to **6**. Using theoretical methods, deeper understanding of electronic effects and molecular structure can be achieved. Thus, appropriate computational methods can be utilized in the design of sensor molecules. Promising candidates can be pre-screened before synthesis and interesting structures can be suggested on the basis of theoretical models. Over all it can be concluded that acceptor-substituted stilbeneboronate pinacol esters introduced in this paper are promising compounds for the colorimetric detection of fluoride ions.

Computational Details

All geometries have been optimized using density functional theory with the B3-LYP functional in combination with the TZVP basis set.^{28,29} The geometries have been converged to a residual gradient norm of 10^{-3} au or better. The energy and density matrix were converged to at least 10^{-6} au, and fine quadrature grids have been used to calculate the exchange and correlation potential (size 5).³⁸ All minima have been characterized by normal-mode analysis. The excitation energies have been calculated using the RI-CC2 method as implemented by Hättig et al.³⁷ For this purpose, the first 10 roots of the electronic hessian have been calculated.

(35) (a) Dreuw, A.; Head-Gordon, M. *Chem. Rev.* **2005**, *105*, 4009–4037. (b) Dreuw, A.; Head-Gordon, M. *J. Am. Chem. Soc.* **2004**, *126*, 4007–4016.

(36) Christiansen, O.; Koch, H.; Jørgenson, P. *Chem. Phys. Lett.* **1995**, *243*, 409–418.

(37) (a) Köhn, A.; Hättig, C. *J. Chem. Phys.* **2003**, *119*, 5021–5036. (b) Hättig, C. *J. Chem. Phys.* **2003**, *118*, 7751–7761. (c) Hättig, C.; Weigand, F. *J. Chem. Phys.* **2000**, *113*, 5154–5161.

(38) Ahlrichs, R.; Bär, M.; Häser, M.; Horn, H.; Kölmel, C. *Chem. Phys. Lett.* **1989**, *162*, 165–169.

Further calculations have been carried out using time dependent density functional theory³⁵ at the B3-LYP/TZVP level of theory. For this purpose, the first 50 roots of the electronic hessian have been calculated. All excitation energies given are low enough to be compared to $-\epsilon_{\text{HOMO}}$, which lies in the order of 6 eV for the noncomplexed species and 3 eV for the complexed species. It should be noted that the computed excitation energies are vertical excitation energies without zero-point energy corrections.

For all of the aforementioned calculations the TURBOMOLE³⁹ program package (for a current version see <http://www.turbomole.de>) has been used. For the interpretation of the electron distribution, NBO analyses⁴⁰ of the Kohn–Sham orbitals have been carried out at the B3-LYP/DZP level of theory⁴¹ using the NBO program as distributed with the NWChem package.⁴²

Experimental Section

X-ray Crystallography. Crystal data of **4** and **6** were collected at room temperature using Mo K α radiation ($\lambda = 0.71073 \text{ \AA}$). Crystal data of **3** and **5** were collected at 100 K using Cu K α radiation ($\lambda = 1.54184 \text{ \AA}$). All structures were solved by direct methods using SHELXS-97.⁴³ All structures were refined by full-matrix least-squares procedures on F^2 , using SHELXL-97.⁴⁴ All non-hydrogen atoms were refined anisotropically. The hydrogen atom positions have been refined with a riding model. In the case of **3** the atoms C33 and C34 have been refined disordered on two positions (C33/C34 and C33a/C34a) with occupation factors of 0.525 and 0.475, respectively. In the case of **4** the atoms O3 and O4 have been refined disordered on two positions (O3/O4 and O3a/O4a) with occupation factors of 0.452 and 0.548, respectively. In case of **6** the atoms C15–C20 have been refined disordered on two positions (C15–C20 and C15a–C20a) with occupation factors of 0.688 and 0.312, respectively. Complete details are available as Supporting Information.

(E)-4-(4,4,5,5-Tetramethyl-1,3,2-dioxaborolan-2-yl)stilbene (3). 4-(4,4,5,5-Tetramethyl-1,3,2-dioxaborolan-2-yl)benzaldehyde (0.400 g, 1.72 mmol) was added to a solution of diethylbenzylphosphonate (0.393 g, 1.72 mmol) in anhydrous DMF (5 mL) under argon atmosphere. Potassium *tert*-butanolate (0.580 g, 5.17 mmol) was added to the clear solution at 0 °C, and the mixture was stirred for 24 h and allowed to warm up to room temperature. The reaction mixture was poured into water (20 mL) and neutralized with 1 M HCl. The white precipitate formed was collected by filtration, washed thoroughly with water, and dried under vacuum. The residue was recrystallized from petrolether to give **3** as colorless needles. Yield: 0.431 g (82%). Mp (petrolether): 123–125 °C. IR (KBr, cm^{-1}): ν 3079, 3025, 2981, 2932, 1604, 1398, 1359, 1327, 1147, 973. ¹H NMR (250 MHz, CDCl_3): δ 1.37 (s, 12H), 7.12 (d, $J = 16.4 \text{ Hz}$, 1H), 7.21 (d, $J = 16.4 \text{ Hz}$, 1H), 7.25–7.32 (m, 1H), 7.33–

7.42 (m, 2H), 7.50–7.63 (m, 4H), 7.83 (d, $J = 8.1 \text{ Hz}$, 2H). ¹³C NMR (62.5 MHz, CDCl_3): δ 24.9, 83.7, 125.8, 126.6, 127.8, 128.6, 128.7, 129.6, 135.1, 137.2, 140.0 (the signal for the carbon atom directly bound to the boron atom is not observed due to the quadrupolar moment of ¹¹B). ¹¹B NMR (80 MHz, CDCl_3): δ 31.0 (br). Anal. Calcd for $\text{C}_{20}\text{H}_{23}\text{BO}_2$ (306.19): C, 78.45; H, 7.57. Found: C, 78.13; H, 7.69. Crystals of **3** suitable for X-ray diffraction were grown by slow diffusion of perfluoromethylcyclohexane into its petrolether solution.

(E)-4-Nitro-4'-(4,4,5,5-tetramethyl-1,3,2-dioxaborolan-2-yl)stilbene (4). 4-(4,4,5,5-Tetramethyl-1,3,2-dioxaborolan-2-yl)benzaldehyde (0.400 g, 1.72 mmol) was added to a solution of diethyl-(4-nitrobenzyl)phosphonate (0.471 g, 1.72 mmol) in anhydrous THF (15 mL) under argon atmosphere. Potassium *tert*-butanolate (0.194 g, 1.72 mmol) was added to the clear solution at room temperature, and the mixture was stirred for 3 h at room temperature. The reaction mixture was filtrated, neutralized with 1 M HCl, and dried with MgSO_4 . After filtration and evaporation of the solvent under reduced pressure, a yellow solid was obtained that was recrystallized from ethylacetate to give **4**. Yield: 0.186 g (31%). Mp (EtOAc): 216 °C. IR (KBr, cm^{-1}): ν 3100, 3070, 2979, 2872, 1632, 1595, 1515, 1358, 1340. ¹H NMR (250 MHz, CDCl_3): δ 1.36 (s, 12H), 7.19 (d, $J = 16.3 \text{ Hz}$, 1H), 7.28 (d, $J = 16.3 \text{ Hz}$, 1H), 7.55 (d, $J = 8.1 \text{ Hz}$, 2H), 7.64 (d, $J = 8.8 \text{ Hz}$, 2H), 7.84 (d, $J = 8.1 \text{ Hz}$, 2H), 8.22 (d, $J = 8.8 \text{ Hz}$, 2H). ¹³C NMR (62.5 MHz, CDCl_3): δ 24.8, 83.9, 124.1, 126.2, 126.9, 127.1, 133.2, 135.3, 138.7, 143.7, 146.8 (the signal for the carbon atom directly bound to boron atom is not observed due to the quadrupolar moment of ¹¹B). ¹¹B NMR (80 MHz, CDCl_3): δ 30.5 (br). Anal. Calcd for $\text{C}_{20}\text{H}_{22}\text{BNO}_4$ (351.19): C, 68.40; H, 6.31; N, 3.99. Found: C, 68.45; H, 6.39; N, 4.03. Crystals of **4** suitable for X-ray diffraction were grown by slow evaporation of an *n*-hexane/ethylacetate solution.

(E)-2,4-Dinitro-4'-(4,4,5,5-tetramethyl-1,3,2-dioxaborolan-2-yl)stilbene (5). 4-(4,4,5,5-Tetramethyl-1,3,2-dioxaborolan-2-yl)benzaldehyde (0.400 g, 1.72 mmol) and 2,4-dinitrophenylacetic acid (0.390 g, 1.72 mmol) were added to anhydrous 1-propanol (5 mL) and heated to reflux for 30 min. To the clear yellowish solution was added piperidine (17 μL), and the mixture was stirred under reflux for 48 h. Upon slow cooling of the reaction mixture, a yellow solid was formed that was recrystallized from *n*-hexane/ethylacetate (1:1 v/v) and dried under vacuum to give **5** as yellow needles. Yield: 0.142 g (21%). Mp (*n*-hexane/EtOAc): 176 °C. IR (KBr, cm^{-1}): ν 3115, 3065, 2983, 2871, 1609, 1531, 1362, 1345, 966. ¹H NMR (250 MHz, CDCl_3): δ 1.36 (s, 12H), 7.28 (d, $J = 16.1 \text{ Hz}$, 1H), 7.56 (d, $J = 8.1 \text{ Hz}$, 2H), 7.68 (d, $J = 16.1 \text{ Hz}$, 1H), 7.85 (d, $J = 8.1 \text{ Hz}$, 2H), 7.98 (d, $J = 8.8 \text{ Hz}$, 1H), 8.43 (dd, $J = 8.8 \text{ Hz}$, $J = 2.3 \text{ Hz}$, 1H), 8.82 (d, $J = 2.3 \text{ Hz}$, 1H). ¹³C NMR (62.5 MHz, CDCl_3): δ 24.9, 84.0, 120.7, 122.1, 126.8, 127.1, 129.0, 135.3, 137.9, 138.0, 138.7, 146.3, 147.4 (the signal for the carbon atom directly bound to boron atom is not observed due to the quadrupolar moment of ¹¹B). ¹¹B NMR (80 MHz, CDCl_3): δ 31.5 (br). Anal. Calcd for $\text{C}_{20}\text{H}_{21}\text{BN}_2\text{O}_6$ (396.19): C, 60.63; H, 5.34; N, 7.07. Found: C, 60.62; H, 5.45; N, 7.26. Crystals of **5** suitable for X-ray diffraction were grown by slow diffusion from *n*-pentane into its ethylacetate solution.

(E)-2,4,6-Trinitro-4'-(4,4,5,5-tetramethyl-1,3,2-dioxaborolan-2-yl)stilbene (6). 4-(4,4,5,5-Tetramethyl-1,3,2-dioxaborolan-2-yl)benzaldehyde (0.400 g, 1.72 mmol, 1.00 equiv) was added to a solution of 2,4,6-trinitrotoluene (0.388 g, 1.71 mmol, 0.99 equiv) in anhydrous toluene (2 mL). The yellowish solution was heated to 80 °C for 30 min, and piperidine (10 μL) was added whereby an orange color appeared instantaneously. The solution was heated at reflux for 4 h, whereupon the solution was allowed to cool to room temperature. The yellow solid formed was filtered, washed with cold toluene, and dried under vacuum. The remaining solution was reduced under vacuum. The resulting solid was filtered, washed with cold toluene, and dried under vacuum. The combined solids were recrystallized from *n*-hexane/ethylacetate (8:5 v/v) and dried

(39) Treutler, O.; Ahlrichs, R. *J. Chem. Phys.* **1995**, *102*, 346–354.

(40) NBO, version 5.0; Glendening, E. D.; Badenhoop, J. K.; Reed, A. E.; Carpenter, J. E.; Bohmann, J. A.; Morales, C. M.; Weinhold, F. Theoretical Chemistry Institute, University of Wisconsin: Madison, WI, 2001.

(41) Dunning, T. H. *J. Chem. Phys.* **1970**, *53*, 2823–2833.

(42) Aprà, E.; Windus, T. L.; Straatsma, T. P.; Bylaska, E. J.; de Jong, W.; Hirata, S.; Valiev, M.; Hackler, M.; Pollack, L.; Kowalski, K.; Harrison, R.; Dupuis, M.; Smith, D. M. A.; Nieplocha, J.; Tipparaju, V.; Krishnan, M.; Auer, A. A.; Brown, E.; Cisneros, G.; Fann, G.; Fruchtl, H.; Garza, J.; Hirao, K.; Kendall, R.; Nichols, J.; Tsemekhman, K.; Wolinski, K.; Anshell, J.; Bernholdt, D.; Borowski, P.; Clark, T.; Clerc, D.; Dachsel, H.; Deegan, M.; Dyall, K.; Elwood, D.; Glendening, E.; Gutowski, M.; Hess, A.; Jaffe, J.; Johnson, B.; Ju, J.; Kobayashi, R.; Kutteh, R.; Lin, Z.; Littlefield, R.; Long, X.; Meng, B.; Nakajima, T.; Niu, S.; Rosing, M.; Sandrone, G.; Stave, M.; Taylor, H.; Thomas, G.; van Lenthe, J.; Wong, A.; Zhang, Z. *NWChem, A Computational Chemistry Package for Parallel Computers*, 4.7; Pacific Northwest National Laboratory: Richland, WA, 2005.

(43) Sheldrick, G. M. *Acta Crystallogr. Sect. A* **1990**, *46*, 467–473.

(44) Sheldrick, G. M. *SHELXL-97, Program for Crystal Structure Refinement*; University of Göttingen: Göttingen, 1997.

under vacuum to give **6** as yellow needles. Yield: 0.596 g (79%). Mp (*n*-hexane/EtOAc): 181 °C. IR (KBr, cm⁻¹): ν 3105, 3078, 2983, 2938, 1605, 1543, 1358, 976. ¹H NMR (250 MHz, CDCl₃): δ 1.36 (s, 12H), 6.76 (d, *J* = 16.5 Hz, 1H), 7.39 (d, *J* = 16.5 Hz, 1H), 7.47 (d, *J* = 8.1 Hz, 2H), 7.83 (d, *J* = 8.1 Hz, 2H), 8.87 (s, 2H). ¹³C NMR (62.5 MHz, CDCl₃): δ 24.8, 84.0, 117.2, 122.2, 126.6, 133.7, 135.3, 137.2, 138.8, 145.9, 150.2 (the signal for the carbon atom directly bound to boron atom is not observed due to the quadrupolar moment of ¹¹B). ¹¹B NMR (80 MHz, CDCl₃): δ 29 (br). Anal. Calcd for C₂₀H₂₀BN₃O₈ (441.183 g/mol): C, 54.45; H, 4.57; N, 9.52. Found: C, 54.45; H, 4.52; N, 9.58. Crystals of **6** suitable for X-ray diffraction were obtained by recrystallization from *n*-hexane/ethylacetate.

Acknowledgment. Financial support by the Fonds der Chemischen Industrie, Frankfurt am Main, and support by the Chemnitz University of Technology is gratefully acknowledged.

Supporting Information Available: Synthesis of **2**, X-ray crystallographic data and collection parameters for **3–6**, ORTEP plots of **3–6**, CIF files of **3–6**, complete list of calculated bond lengths between non-hydrogen atoms, UV–vis spectroscopical data and calculated binding isotherms, Cartesian coordinates for all geometry-optimized species, and ¹H and ¹³C NMR spectra for **3–6**. This material is available free of charge via the Internet at <http://pubs.acs.org>.

JO070084V